PREDICTING THE MINERALOGY OF VESTA USING BOTH METEORITIC AND SYNTHETIC SAMPLES

by

Katelyn Marie Lehman

Submitted in partial fulfillment of the
requirements for Departmental Honors in the
School of Geology, Energy, and the Environment
Texas Christian University
Fort Worth, Texas

May 2, 2014

PREDICTING THE MINERALOGYOF VESTA
USING BOTH METEORITIC AND
SYNTHETIC SAMPLES

Project Approved:

Supervising Professor: Rhiannon Mayne, Ph.D.
School of Geology, Energy, and the Environment

Arthur Busbey, Ph.D.
School of Geology, Energy, and the Environment

Liran Ma, D.Sc.
Department of Computer Science

ABSTRACT

The second largest asteroid, Vesta, tells an important story. This differentiated body gives a look at early planet formation, and consequently how a young Earth formed. Much of the process of how young bodies differentiate is unknown. If we analyze this body and understand the relationship between the different rock types then we can begin to understand differentiation. Geologically on Earth we do this by examining an outcrop, mapping, and doing chemical analysis on the different rocks. In space, the tools for analysis are more limited. The primary tool for understanding an outcrop is through remote sensing data with spectral analysis being the primary tool to understanding composition. The problem with spectral data is that it needs groundtruthing and to groundtruth, one must have samples. Luckily, in the case of Vesta, there are samples available through meteorites. In this study, Vestan minerals' spectral data was calibrated (groundtruthed) in order to accurately predict mineralogy on Vesta.

ACKNOWLEDGEMENTS

Thank you TCU community for giving me this amazing adventure.

Special thanks go to my advisor and mentor, Dr. Rhiannon Mayne. Thank you for introducing me to the planetary world. You opened my eyes not just to the Universe around me, but also to my own potential. Your unending support and inspiration means so much to me.

Thank you, Dr. Nowell Donovan, for inspiring me in my first geology class and opening up the world of research to me. Thank you for your amazing positivity and thoughtful guidance. You pushed me to be the leader I have become.

TCU professors and staff are true mentors. Guiding, supporting, and forming an intimate community. I could not have chosen a better place to attend for my Undergraduate degree. Thank you. To name a few of these special people: Terri Mabe, Dr. Richard Hanson, Dr. Art Busbey, Dr. Art Ehlmann, Dr. Liran Ma, and Dr. Tony Burgess. I hope to inspire just as you have as I pursue my goal to be a professor.

My deepest appreciation goes to my family. To my hilarious and uplifting older brother, my generous and dedicated mother, and my involved and comedic father, I cannot express how deeply grateful I am to have such amazing love and support. My Aunt Breda and Uncle George, thank you for bringing me into your home and supporting all my academic endeavors. I value all the time we have spent together.

TABLE OF CONTENTS

INTRODUCTION 1

BACKGROUND 1

Howardite, Eucrite, and Diogenite Meteorites 3

Previous Studies 3

Pyroxene Crystal structure and Relationship to Reflectance Spectra 4

Modified Gaussian Model 6

Deriving Cooling History and Geothermometry from Pyroxenes 7

THE IMPORTANCE OF UNDERSTANDING THE PETROLOGY OF VESTA 8

METHODS 10

RESULTS 11

DISCUSSION 13

CONCLUSION 16

APPENDIX 17

REFERENCES 32

INTRODUCTION

Looking upon the night sky, most people cannot help but be filled with amazement. The breadth and beauty of space, and all the scientific possibilities it contains, binds each person in this world together. One cannot help but ask: what lies in that great beyond that we call the Universe? Perhaps, though, the more quintessential question is, how did the Earth form in this universe?

To answer this question, one must study the materials that originally formed the Earth and how key Earth features formed, such as the Earth's layers. Unfortunately, the Earth's tectonic processes are consistently destroying old and generating new crustal materials, eliminating all the evidence of young Earth materials. Fortunately, we can gain much of the information about the early Earth from planetary body analogs: asteroids.

BACKGROUND

Asteroids are rocky bodies that were accreted in the early Solar System. Asteroids are considered to be either differentiated or undifferentiated. Undifferentiated asteroids are defined by their lack of melting and lack of major compositional evolutions. These undifferentiated bodies describe the earliest stages of planet formation and can be studied to explain how Earth first accreted. Differentiated asteroids are bodies that have melted and formed distinct compositional layers. This process is called differentiation, hence the type of asteroid. Unlike the Earth, these differentiated materials have preserved the composition and thickness of their original layers formed ~4.56 billion years ago, providing a snapshot of a body quickly after differentiation.

One such asteroid is 4-Vesta. With a mean radius of 258km, Vesta is the largest differentiated asteroid in our Solar System, representing an early phase of planet formation (McCord *et al.*, 1970; Binzel; 1997) (Figure 1). The differentiated body represents a near-perfect analog to a young Earth before tectonic processes (McCord *et*

al., 1970; Binzel; 1997) (Figure 2). Thus, if the geology and geologic history of Vesta can be garnered, then the processes that formed our layered young Earth can be deduced.

How can we discern the geology of Vesta? The petrology of planetary bodies can be studied primarily by means of spacecraft data and physical samples, with spacecraft data being the most accessible form. In 2007 the Dawn Mission launched with the goal of understanding Vesta's geology (Russell *et al.*, 2004). The Dawn space craft has four instruments: a framing camera, a visible-infrared mapping spectrometer, a magnetometer, and a gamma ray and neutron spectrometer (Russell *et al.*, 2004). These four instruments work together to map the surface of Vesta. The main instrument used to distinguish composition is the spectrometer which obtained visible to infrared (VIS-NIR) spectra (Russell *et al.*, 2004 and 2005). Spectral analysis is one of the most accessible methods to analyze planetary bodies' mineralogy and it works by describing how a mineral interacts with light. Depending on how the light is absorbed and reflected, the type of mineral can be identified. To be able to identify minerals based on their spectra, there needs to be a basis to perceive the spectral signature of each mineral. In other words, a representative sample and spectra is needed for each type of mineral being analyzed. Spectral analysis is not perfect, though. Not all minerals have strong spectral signatures and the surfaces being analyzed are not simply one type of mineral. The surfaces are made of rock, a mixture of minerals. Thus, the spectral signature of the rocky surface is formed from a mixture of the different minerals' spectra on that surface. Unfortunately, though, the resultant spectra is not a linear mixture of the minerals. Thus, the correspondence between minerals, their spectra, and the resultant spectral mixtures they can form needs to be established. The data must be calibrated (groundtruthed). Yet the current mode to interpret the Vestan spectra is based on Earth-composition mineral calibration (Sunshine and Pieters, 1993), which has been shown to be inaccurate (Mayne *et al.*, 2010; Beck *et al.*, 2011).

Howardite, Eucrite, and Diogenite Meteorites

Fortunately, Vesta has a group of associated meteorites: the howardite, eucrite, and diogenite group (HEDs) which can be used to calibrate the spectral data (McCord et al, 1970, Mayne *et al.*, 2009, McSween *et al.*, 2011) (Figure 2). The eucrites are basaltic, the diogenites are ultramafic orthopyroxenites, and the howardites are breccias (mixtures) of eucrites and dioginites formed by impact (Mittlefehldt *et al.*, 1997; Beck *et al.*, 2011). Each type of meteorite is considered to be a part of a distinct layer on Vesta and an abundance of geologic information can be garnered about Vesta from these meteorites, such as age (Haack, 1990; Eugster and Michel, 1995; Kleine *et al.*, 2004, Wadhwa *et al.*, 2006, McSween *et al.*, 2011), geochemistry (McSween *et al.*, 2011), and possible formation history (Mayne *et al.*, 2009, McSween *et al.*, 2011). The problem is that there is no geologic context. It's merely a guessing game as to where each of these HEDs came from on Vesta. Thus, there needs to be a way to determine the distribution of these meteorites on Vesta. Luckily, as discussed earlier, the Dawn mission is currently mapping the surface and obtaining spectra that correlates with the composition of Vesta. If the spectral data can be correlated with that of the meteorites, the geology of Vesta can be understood (Mayne *et al.*, 2010).

Previous Studies

Mayne *et al.* (2010) showed through performing spectral analysis on eucrites with known compositions (Mayne *et al.*, 2009) that plagioclase, olivine and pyroxene can be identified from Vestan spectra using an Earth-based calibration. Pyroxene, a silicate with varying amounts of magnesium, iron, and calcium, dominates the Vestan spectra and the composition of that pyroxene is indicative of thermal history. The partitioning of both major (Ca^{2+}, Mg^{2+}, and Fe^{2+}) and minor (Ti^{4+}, Al^{3+}, Cr^{3+}) cations in pyroxene is vital to perceiving the degree and history of magmatic evolution (Adam, 1974; Cloutis and Gaffey, 1991a and 1991b, Pun and Papike, 1996, Sunshine and Pieters, 2004, Mayne *et al.*, 2009). The Modified Gaussian Model (MGM) can be used to anticipate these cation

locations. MGM uses an algorithm to deconvolve spectral mixtures into distinct absorption bands which can be correlated directly with minerals and even the cation locations in those minerals(Sunshine, 1990; Sunshine and Pieters, 1993). Mayne *et al.* (2010) showed that much of the pyroxene composition could be derived from the spectra using MGM and then the Earth-based calibration, and a qualitative understanding of cation locations could be understood, but the ratio of low calcium pyroxene to high calcium pyroxene (HCP/ (HCP+LCP)) was inaccurately predicted (±9%) (Sunshine and Pieters, 1993). This ratio is important, because the amount of HCP can indicate the igneous history (Sunshine and Pieters, 2004).

When a primitive (unmelted) body, like an asteroid, undergoes differentiation the amount of high-calcium pyroxene (HCP) relative to low-calcium pyroxene (LCP) present changes depending on the degree of melting (Sunshine and Pieters, 2004). This makes the ratio of HCP to LCP (HCP/ (HCP+LCP)) a very important factor for interpreting planetary surfaces.

Why is the Earth-based calibration so ineffective in analyzing the Vestan pyroxenes? Vestan pyroxenes are much higher in iron, which considerably changes the spectral signature. To effectively predict the HCP to LCP ratio from Vesta's spectra, the data must be calibrated to Vestan-composition pyroxenes. Since spectra are derived from light's interaction with the crystal structure, and are affected by the type and amount of cation, it is important to first understand how variation in the crystal structure alter the spectral signature.

Pyroxene Crystal structure and Relationship to Reflectance Spectra

Knowledge of pyroxene crystal structure is fundamental to differentiating pyroxene reflectance spectra (Figure 3).

Pyroxenes are Fe-Mg- rich chain silicates separated into two main groups: low-calcium pyroxenes and high-calcium pyroxenes (Burns, 1993). There are two main octahedral cation sites in all types of pyroxenes, referred to as M1 and M2 (Figure 4).

These sites contain a transition metal surrounded by a ligand field made up of oxygens. The M1 site is smaller and more symmetric, than the M2 site. The reflectance spectrum of pyroxenes is dependent on the symmetry of the ligand field of these cation sites, which is effected by the transition metal contained within the cation site and the geometry of the site. An asymmetric ligand field causes the transition metal's *d*-orbital to split into a lower energy suborbital and a higher energy suborbital. When a photon interacts with this now split crystal field, it can be absorbed causing a lower energy electron to jump to the higher energy suborbital. Assuming the electronic transition is spin-allowed, a strong absorption is produced which can be observed in the spectra.

In pyroxenes, both the M1 and M2 sites produce these prominent spin-allowed absorptions (Burns, 1993; Klima, 2007). The M2 site's large size causes Fe^{2+} and Ca^{2+} to preferentially fill the M2 site producing two strong spin-allowed absorptions at ~1 μm and ~2 μm. Since Ca^{2+} is larger than Fe^{2+}, the cation fills the M2 site first. When Ca^{2+} replaces Fe^{2+} or the M2 site is saturated with Fe^{2+}, the Fe^{2+} is pushed into the M1 site creating a spin-allowed ~0.9μm absorption. As Fe increases in the M1 site, two additional spin-allowed absorptions are formed with absorption band centers at ~0.75 μm, and ~1.2 μm (Klima *et al.*, 2010). Thus, a ~0.75 μm, and ~1.2 μm absorption observed in a spectra indicates either a high-Fe^{2+} pyroxene of a Ca^{2+} saturated pyroxene.

Minor elements including Ti^{4+}, and Cr^{3+} can be present in the M1 site creating distinct absorptions(Adams, 1974; Burns, 1993). Presence of Ti^{4+} can cause a spectra to shift to longer wavelengths and creates an absorption around ~0.75 μm (Adams, 1974). Cr^{3+} creates a ~0.6μm absorption (Rossman, 1980; Burns, 1993; Mayne *et al.*, 2010. Beyond the metal-ligand field geometry, the pyroxene chain geometry also contributes to absorption locations.

Low calcium clinopyroxenes (LCP), compared to high calcium clinopyroxenes (HCP) have distinct geometric differences which results in shifts of the wavelength in which absorptions occur. LCP at high temperatures are part of the C2/c space group, but

as they cool their structure becomes unstable causing the C2/c space group to reorient into the P21/c space group (Burns, 1993; Klima *et al.*, 2010). This transition into a different space group creates a highly kinked chain of octahedrals (Figure 5) (Cameron and Papike 1980, Klima, 2010). HCP is a part of the C2/c space group, both in high and low temperature, and forms a very straight chain of octahedrals. LCP's kinked chain shifts spectra to shorter wavelength than its HCP counterparts.

Pyroxenes have distinct observable absorptions which describe the crystal structure and the amount of cations forming the mineral. Thus, if the resultant spectra can be separated (deconvolved) into these specific absorptions, then the type of pyroxene, and consequently the HCP to LCP ratio, can be discovered.

Modified Gaussian Model

Spectroscopy is a key tool for interpreting the mineralogy and geologic history of planetary bodies, but to ascertain that history and mineralogy, the spectra must be deconvolved into distinct absorption bands. These distinct absorptions in the VIS-NIR caused by how light interacts with the pyroxene structure can be located using the Modified Gaussian Model (MGM) and are fundamental to understanding the proportion of a type of mineral in the surface analyzed. The mathematical Modified Gaussian Model (MGM) achieves this through successfully modeling the physical processes required to form an electronic transition absorption (Sunshine *et al.*, 1990).

While early studies showed that these absorptions could be deconvolved into discreet Gaussian distribution, MGM modifies the shape of the Gaussian distribution by attributing the randomness variable to average ion-ligand bond length, and thus, the distortion of the M1 and M2 sites (Sunshine *et al.*, 1990). This enables one modified Gaussian distribution to represent one absorption band (Sunshine *et al.*, 1990). This is important because modeling every absorption band with simply one modified Gaussian distribution, MGM creates a more effective mineral identification tool that does not require endmember knowledge.

MGM describes an absorption band through its band center (μ), band width (σ), and band strength (*s*) (Equation 1).

Equation (1)

$$m(x) = s \cdot \exp\left\{\frac{-\left(x^{-1}-\mu^{-1}\right)^2}{2\sigma^2}\right\}.$$

The summation of these discrete absorption bands forms the reflectance spectrum (Sunshine *et al.*, 1990). Once the cation location and proportions are derived via deconvolution, the melting history of that pyroxene can be inferred.

Deriving Cooling History and Geothermometry from Pyroxenes

The partitioning of the major cations in pyroxene gives information about the magma cooling history and magmatic evolution. The cooling history of a lithology can be determined based on the distribution of Fe^{2+} and Ca^{2+} in the M1 site (Virgo and Hafner, 1970; Saxena *et al.*, 1974; Lindsley, 1983; Anovitz *et al.*, 1988; Molin and Zanazzi, 1991; Klima, 2008). As previously described, the M1 site when either saturated with Ca^{2+} or high in Fe^{2+} produces a distinct 1.2 μm absorption band. Klima (2008) showed that the ratio of the 1.2μm band's strength to the 2μm band (M1 ratio intensity) can be used to resolve the cooling rate. Klima (2008) determined this M1 ratio intensity commonly was ~0.1 μm to ~0.4 μm for HED meteorites with slowly cooled pyroxenes forming a weaker 1.2μm absorption and a smaller M1 ratio intensity, and quickly cooled pyroxenes having a stronger 1.2μm absorption band with a larger M1 ratio intensity.

The degree of magma evolution can be surmised by the HCP/(HCP+LCP) ratio derived from the component band strength ratio where

Equation (2)

CBSR= Band Strength of the LCP component/ Band Strength of HCP component.

(Sunshine and Pieters, 1993; Sunshine *et al.*, 2004). The metal-ligand derived absorptions band strengths which are used to resolve the ratio of high-calcium pyroxene to low calcium pyroxene in terrestrial pyroxenes can be used to figure out the degree of

melting and differentiation from a primitive ordinary chondritic body (Sunshine *et al.*, 2004; Mayne *et al.*, 2010). A primitive achondrite (an unmelted asteroid) has a HCP/(HCP+LCP) less than 0.10, while a that HCP/(HCP+LCP) greater than 0.30 indicates 30% partial melting of the original primitive material (Sunshine *et al.*, 2004). A high HCP/(HCP+LCP) requires extensive differentiation of an asteroid (Sunshine *et al.*, 2004).

Minor element variation can also be used to postulate magma evolution. Mayne *et al.* (2009) revealed there were minor element variations in the HED pyroxenes with Cr^{3+}, Al^{3+}, and Ti^{3+} representing different stages of differentiation (Pun and Papike, 1996). Mayne *et al.* (2010) showed that those same Cr-rich eucrites had a strong ~0.6 um Cr^{3+} absorption and that the percent of Cr^{3+} could be predicted to ± 0.26% from the absorption band strength via the equation by Cloutis (2002). Cr^{3+} is a compatible element in pyroxene becoming incorporated into the M1 site and indicates a primitive Cr-rich melt (Mayne *et al.*, 2010; Pun and Papike, 1996). As the melt evolves and Cr-rich pyroxenes crystallize out, Al concentration increases (Mayne *et al.*, 2010; Pun and Papike, 1996). Al-rich pyroxene crystallizes out until plagioclase can crystallize, the plagioclase then incorporates the Al^{3+}, and the melt becomes enriched in Ti^{3+}, which later forms Ti-rich pyroxene and opaques (Mayne *et al.*, 2010; Pun and Papike, 1996).

Being able to identify the presence and proportion of cations is crucial to understanding the geologic history of Vesta.

THE IMPORTANCE OF UNDERSTANDING THE PETROLOGY OF VESTA

The knowledge of the petrology of Vesta is important because it can be used to explain how the whole body differentiated and consequently how protoplanets differentiate. This information comes from a combination of petrologic and thermal information. Studies of HEDs have supplied a wealth of information of different petrologies on Vesta and led to two main formation methods (Haack, 1990, Gosh and McSween, 1992; Kleine *et al.*, 2004; Sunshine *et al.*, 2004; Mayne *et al.*, 2009, McSween

et al., 2011). Either fractional crystallization (Mason, 1962; Righter and Drake, 1997; McCoy *et al.*, 2006) or partial melting (Stopler, 1977; Gosh and McSween, 1998; McCoy *et al.*, 2006) could have formed Vesta and its resultant petrologies.

It has been suggested that Vesta formed via fractional crystallization through a magma ocean formation model (Ruzicka *et al.*,1997) or equilibration crystallization of a large molten body with fractional crystallization after convective lockup (Righter and Drake, 1997). Both models begin with a large molten body, as it cools, in the case of the magma ocean model diogenites form a cumulate pile and eucrites form from continued fractional crystallization of the residual melt (Ruzicka *et al.*, 1997). This would create a laterally, compositionally homogenous Vesta with the crust made up of 23-42 km of eucrite and 12-43 km of the ultramafic diogenites making up the upper mantle and lower crust (Ruzicka *et al.*, 1997). This structure could be seen in the spectra if the HCP to LCP ratio was known. If the distribution of HCP to LCP is laterally homogenous and forms thick vertical layers with different HCP values (Sunshine *et al.*, 2004; Mayne *et al.*, 2010).

In the case of equilibrium crystallization model, the magma ocean is convecting. In this convecting magma ocean, there is continual equilibrium crystallization until there is convective lockup due to cooling. After lockup, equilibrium crystallization can no longer occur, so the residual magmas are fractionally crystallized (Righter and Drake, 1997). This would produce a 10-15 km thick basaltic crust, with the orthopyroxenite digogenites underneath (McCoy *et al.*, 2006). Similarly, this structure is identifiable if the HCP:LCP ratio is known. The HCP to LCP distribution would also be laterally homogenous, but the layers would be thinner, as would be visible from crater thickness calculations (Sunshine *et al.*, 2004; Mayne *et al.*, 2010)

On the other hand, Vesta could have formed from the partial melting of accreted ordinary chondritic material and the HEDs and other materials would be a result of melts derived from this initial material. Partial melting would form magma chambers that were

thick in the shallow crust and widespread and thin in the deep crust (Wilson and Keil, 1996; McCoy, 2006). In this case, the HCP: LCP ratio distribution would be highly heterogeneous both laterally and vertically.

Vesta's spectra contains vital information about early planet formation and much of that information can be derived from HCP/ (HCP+LCP) ratio. Based on the distribution of HCP:LCP, the formation of Vesta can be gleaned.

METHODS

The goal of this study is to effectively calibrate Vestan pyroxene spectra utilizing MGM. This calibration would enable the CBSR to be accurately resolved, and thus, the HCP to LCP ratio. Eucrite pyroxene compositions were used to determine the pyroxene end-member compositions that could be found on Vesta. The pyroxene end members would have a higher Fe content than the related terrestrial pyroxenes. Employing this information, Don Lindsley of SUNY-Stony Brook, New York synthesized two pyroxenes, a high calcium, high iron pyroxene and a low calcium, high iron pyroxene, $Wo_{40}En_{30}Fs_{30}$ (HCP) and $Wo_{3.50}\ En_{35}\ Fs_{61.5}$, respectively, where Wo represents wollastonite ($Ca_2Si_2O_6$) , En represents enstatite ($Mg_2Si_2O_6$) , and Fs for ferrosilite ($Fe_2\ Si_2O_6$) (Figure 6). These spectra represent the HCP and LCP end members, i.e. 100% HCP and 100% LCP.

In the process of synthesizing these pyroxenes, water must be incorporated into the silicate. This water can at times hydrate the pyroxene forming amphibole. An X-ray Diffractometer (XRD) confirmed that amphibole had not been created, and that the samples were, indeed, pure (Figure 7).

The synthesized pyroxenes were then sieved to <45 microns dry powders. The goal being to reduce the effect of grain size on spectra (Sunshine and Pieters, 2003). These endmembers were then used to create mechanical mixtures. The mixtures produced included 25% LCP-75% HCP (25LCP75HCP), 50% LCP-50% HCP (50LCP50HCP), 75% LCP-25% HCP (75LCP25HCP).

The endmember pyroxenes and the three mixtures were then sent off to the Reflectance Experiment Laboratory (RELAB) at Brown University for spectral analysis. The spectral analysis is comparable to that of the instrumentation of the Dawn spacecraft and the data it can obtain (Pieters *et al.*, 2004; Russel *et al.*, 2004 and 2005). Thus, the spectra obtained from the synthetic pyroxenes and pyroxene mixtures are consistent with the spectral signatures on Vesta. We can use spectra of the synthetic pyroxenes to calibrate the spectra tools used to analyze Vesta.

The synthetic pyroxene spectra were calibrated using MGM. The endmembers were first modeled by systematically adding bands to describe the major cation locations. The stochastic inversion method was used to create reasonable bounds for the band centers, band widths, and band strengths (Tarantola and Valette, 1982; Sunshine and Pieters, 1993). The RMS error is utilized as tool to ensure the fit, and clarify if bands are missing (Sunshine and Pieters, 1993). Similarly the mixtures were modeled beginning with a one-pyroxene model and adding additional bands to accurately describe the two-pyroxene model.

The known HCP/ (HCP+LCP) ratio was then calibrated to the now deconvolved pyroxene mixtures by calculating the component band strength ratio (CBSR) (Equation (1)) (Sunshine and Pieters, 1993). This ratio was calculated for both the 1μm and 2μm bands. These known ratios to the CBSR were then plotted and calibration was derived for predicting HCP to LCP from the CBSR (band ratios).

This calibration was then be applied to the spectra of chemically know eucrite meteorites analyzed by Mayne *et al.* (2009) and Mayne *et al.* (2010) to clarify the calibration.

RESULTS

XRD analysis clarified the purity of the synthesized endmembers, $Wo_{40}En_{30}Fs_{30}$ (HCP) and $Wo_{3.5}En_{35}Fs_{61.5}$ (LCP) by ensuring that they did not contain the characteristic strong 10° emission of amphibole (Figure 7) (Burns, 1993).

RELAB spectral analysis produced five distinct spectra for the two endmembers and three mixtures.The LCP endmember was modeled with seven absorption bands (Figure 8, Table 1). The HCP endmember were modeled effectively using 7 absorption bands (Figure 8, Table 1). Figure 8 show a relatively flat rms error with a straight continuum, supporting the validity of these fits. The band parameters shown in Table 1 were as expected based on the high amount of iron in both endmember. The terrestrial pyroxene spectra differs greatly from the Vestan pyroxene spectra with additional bands and change in depth with increase in iron (Figure 8, Figure 9). The LCP Vestan endmember is much higher in iron than terrestrial LCP. The increase in iron would push more iron into the M1 site. As more iron replaces magnesium in the M1 site two bands are produced, one around 0.90 μm and one approximately at 1.2μm. These two bands are apparent in both the Vestan LCP and Vestan HCP spectra. The LCP spectra also contains the two characteristic absorptions produced from iron in the M2 site located approximately at 1 and 2 μm, and a water band at approximately 2.6 μm. The Vestan HCP differs from the LCP as the increase in calcium content causes the spectra to shift to longer wavelengths (Table 2). The HCP is also lacking the water band and has smaller 1 and 2 μm band strengths.

The mixtures were all modeled initially as one-pyroxene (HCP) and then additional bands were added to effectively fit the spectra. All mixtures were modeled effectively with the same two-pyroxene mixture model which deconvolved the spectra into 9 bands (Figure 10, Figure 11, Figure 12). These 9 bands (Table 2) have an additional 1 μm band and a 2 μm band, and also need a require a water band for an effective fit.

While the band center of the all bands shifts to longer wavelength with calcium increase, more noticeable are the differences in band depth between the endmembers and different mixtures (Figure 13). When related to the known HCP/(HCP+LCP) of the synthesized Vestan pyroxene mixtures, CBSR forms a smooth negative continuum (Figure 14).

This can be approximated by relating HCP/(HCP+LCP) to CBSR both logarithmically or linearly (Figure 15). This relationship was then tested using the spectra of known composition eucrites in an effort to see if the calibration would effectively predict the HCP to LCP on Vesta. Mayne *et al.* (2010) applied MGM to nine eucrite spectra in an effort to analyze the effectiveness of Earth-based spectral calibration and garner additional mineral-spectra relations to be applied to the spectra of Vesta. The nine eucrites and their predicted spectral mineralogies are detailed in Table 3. The deconvolution results of Mayne *et al.* (2010) were employed to test the effectiveness of the new Vestan-calibration.

The CBSR was calculated for each of the nine unbrecciated eucrites for both the 1μm and 2 μm absorption bands utilizing the results of Mayne *et al.* (2010). The CBSR of each meteorite was compared to the percent of HCP to LCP (Figure 16). The calibration was then applied to the CBSR and the predicted HCP to LCP ratio was compared to the known value. The resultant HCP/(HCP+LCP) predicted by the new calibration was shown to be inconsistent with known values. The calibration predicted much lower percentages of high calcium pyroxene (Table 4). The synthetic pyroxene's CBSR-HCP to LCP relationship was plotted alongside the known eucrite CBSR-HCP to LCP relationship in an effort to understand how the calibration differed from the known eucrite compositions (Figure 17). The deconvolution was rechecked to ensure the validity of the fit.

DISCUSSION

To conceive why the calibration proved the scientific process was thoroughly examined. There could be three major causes for the ineffective calibration the MGM fits were invalid, the mixtures were not thorough mixed, thus the calibration base is inaccurate, or their are additional factors that are affecting the spectra of the synthetics such as grain size. The MGM fits, themselves, appeared accurate for three reasons. First, the fits had relatively flat RMS errors, indicating that the fit did not require additional

bands to be added. To ensure this was not the case, additional bands were added to see if the result was more effective in predicting the HCP percentage. Although, additional bands can always be added to the spectra, mathematically the most effective fit is the one using the least number of bands to describe the spectra (Sunshine et al., 1993; Mayne et al., 2009). Despite, this knowledge, the spectra was fit with additional absorption bands that appeared in the endmembers. The additional band fits proved even more ineffective. This calibration was highly erratic predicting highly variable percentages of high calcium pyroxene that were even lower than predicted by the first calibration. Secondly, the CBSR-HCP/(HCP+LCP) relationship for the three mixtures formed a smooth continuum. This would suggest that the fit was correct and that indeed the mixtures are correct. Furthermore, the same two pyroxene fit was able to be applied to all three mixtures. This implies that this is a highly effective fit and that the mixtures band depths are correlated in the same way for each mixture.

When deciding whether these mixtures were not mixed properly, the five spectra are compared. The band center shifts steadily between the HCP to LCP range. This would suggest that indeed the mixtures are correct, but to fully test this, more detailed chemical analysis would need to be completed.

The final plausible cause for the calibration error is the spectral effect of grain size. As you change grain size, the spectral signature also changes with band depth decreasing when the grains are smaller than 45 μm, and the relationship (ratio of band strengths) changing between absorption bands (Sunshine et al., 1993). Mustard and Hayes (1997) showed that even smaller particles effect the spectral relationships even more dramatically. There is a definitive relationship with a decrease in particle size below 45μm and a change in the band relationships. Absorptions' band depths remain the same at some wavelengths despite the change in size, while other shift or decrease in depth (Mustard and Hayes, 1997). In the case of this study, the original grains were quite small and easily fell through the 45μm screen when sieved. This indicates that many particles in

the mixture were smaller than 45 μm. This would explain why the CBSR relationship is so different between the synthetic samples and the eucrite samples. To correct this in the next study, larger grain size pyroxene must be produced.

If the effect is based on grain size, the fit could still be effective, even though the calibration was not. To correct the calibration, new mixtures with a larger grain size must be produced. To increase the statistical correlation a larger range of mixtures also need to be created such as a 15% HCP, 85% LCP, etc. This will make the new calibration statistically more accurate. The fit previously found, if effective, indicates that the grain size was indeed the primary error in this study.

Although the calibration was not effective, this study was able to verify many things about Vesta's pyroxenes. It showed how dramatically the high amounts of iron change the spectra of Vestan pyroxene from that of terrestrial pyroxenes. The M1 and M2 become absolutely filled with iron and calcium. Alongside creating deep M2 absorptions and changing band center location. These high iron pyroxenes create dramatic M1 absorptions at 0.9μm and 1.2μm. The assertions of Klima (2008) that the 1.2μm band can be used to derive the cooling rate is important when applying those cooling rates to Vestan pyroxenes. If the band depths of the 1.2μm region are not as deep as those observed in the synthetic pyroxenes, then based on the study by Klima (2008) the pyroxenes would have cooled much slower than the lab pyroxenes used in this study. An additional study could be made using the relationship derived by Klima (2008) to acquire the amount of time required to cool pyroxenes varying 1.2μm/2μm band depth ratios.

This study also brings up the question of the effects of grain size on these planetary bodies being analyzed. Most planetary body surfaces have grain sizes below <45μm. So, how effective are our calibrations if they are based off of higher grain size calibrations? An additional study could be performed finding a more effective HCP to LCP indicator that is unaffected by grain size.

CONCLUSION

The new influx of spectral data of Vesta brings a wealth of new information that can be used to understand the geologic history of the body. Vesta's spectra holds vital information about early planet formation and much of that information can be derived from HCP/ (HCP+LCP) ratio. HCP acts as an igneous tracer with high HCP indicating either early stages of differentiation or extensive differentiation (Sunshine *et al*., 2004). The distribution of that HCP in relation to LCP is key to determining the formation method of Vesta. If the distribution of HCP to LCP is laterally homogenous and forms thick vertical layers with different HCP to LCP ratios it may support a magma ocean formation model or equilibration crystallization of a large molten body with fractional crystallization after convective lockup (Ruzica *et al.*, 1997; Righter and Drake, 1997; McCoy *et al.*, 2006; Mayne *et al.*, 2010). On the other hand, if the distribution of HCP to LCP is laterally heterogeneous, then Vesta's different petrologies could be a result of partial melting (McCoy *et al.*, 2006; Gosh and McSween, 2008; Mayne *et al.*, 2010). The percentage of iron and calcium in the various pyroxene metal-ligand sites can indicate the rate of cooling. As of yet, though, the calibrations have been ineffective in predicting that percentage.

This study worked to more effectively evaluate the Vestan spectra for the HCP/(HCP+LCP) ratio by using synthetic Vestan pyroxene mixtures to model the spectra. Two endmembers and three mixtures were formed and analyzed (75% HCP 25% LCP, 50% HCP 50% LCP, 25% LCP 75% HCP). While both the mixtures and the endmembers could be effectively modeled, and the fits appeared accurate, the calibration was ineffective. More mixtures must be made so that the relationship between CBSR and HCP/ (HCP+LCP) can be made. This study is the first step in more effectively determining how Vesta formed.

APPENDIX

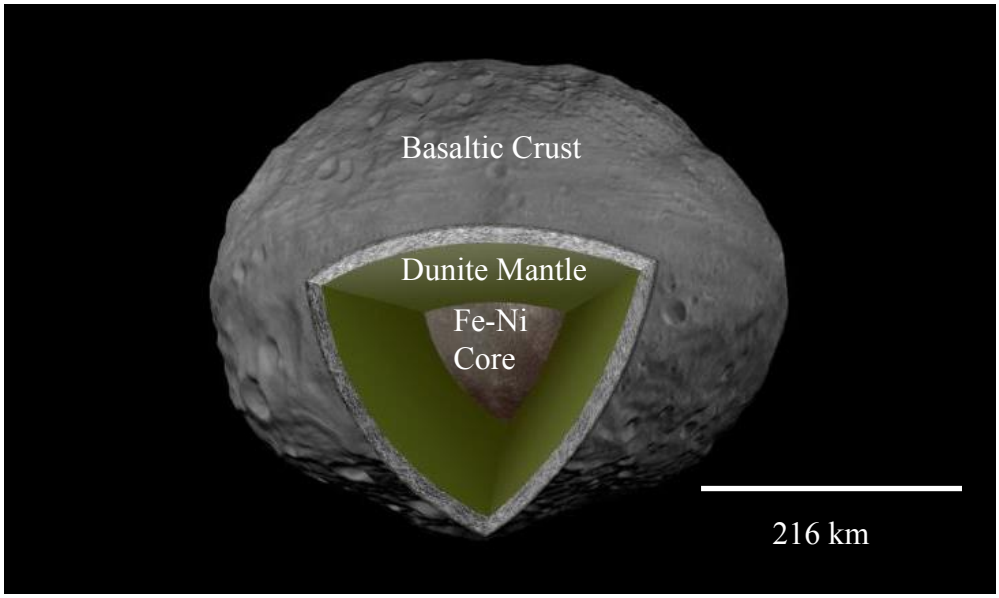

Figure 1: Using composite images and topography of Vesta from Dawn, this artist renders an image of the potential internal structure of Vesta. Showing a core, mantle, and crust. *Image Credit: NASA/JPL-Caltech*

Figure 2: The HED group can be used to groundtruth spectral data of Vesta. These three images show examples of members of the HED group including a slice of a howardite from Kapoeta, Sudan, a eucrite from Kirbyville, TX, and a diogenite from Bilanga, Barkina Faso. These three meteorites are housed in the Monnig Meteorite Collection. *Image credits: Oscar E. Monnig Meteorite Collection.*

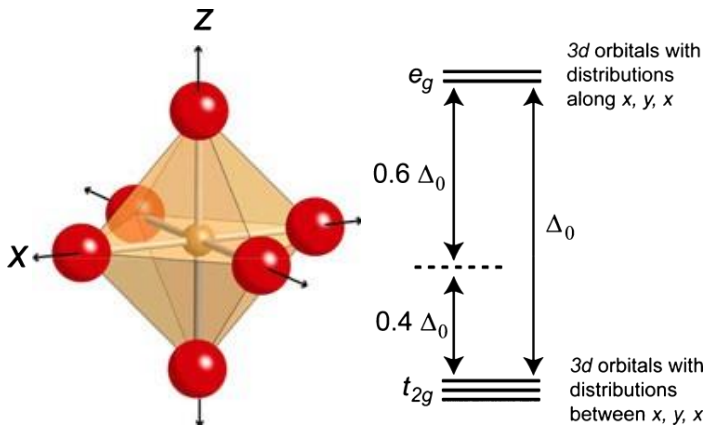

Figure 3: From Klima (2008), this idealized pyroxene octahedral site. When Fe enters the central metal site it changes the symmetry of the octahedral causing a splitting of the crystal fields. The crystal field splitting diagram is also shown.

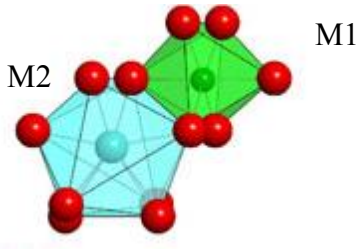

Figure 4: Modified from Klima (2010), this shows the configurations of crystal structures. The M2 site (blue) is larger and more assymetric, and the M1 site is smaller and very symmetric.

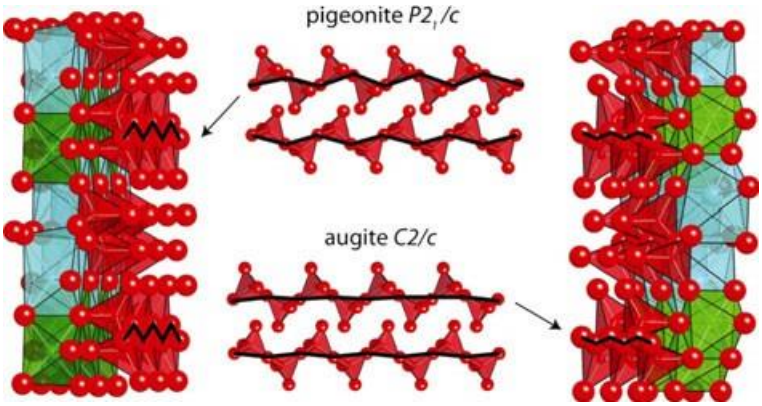

Figure 5: From Klima (2010), this illustration portrays the effects of changing spaces groups. As the high temperature C2/c space group pyroxenes cool there structure changes creating kinked chains. Low calcium pyroxenes display this characteristic kinking.

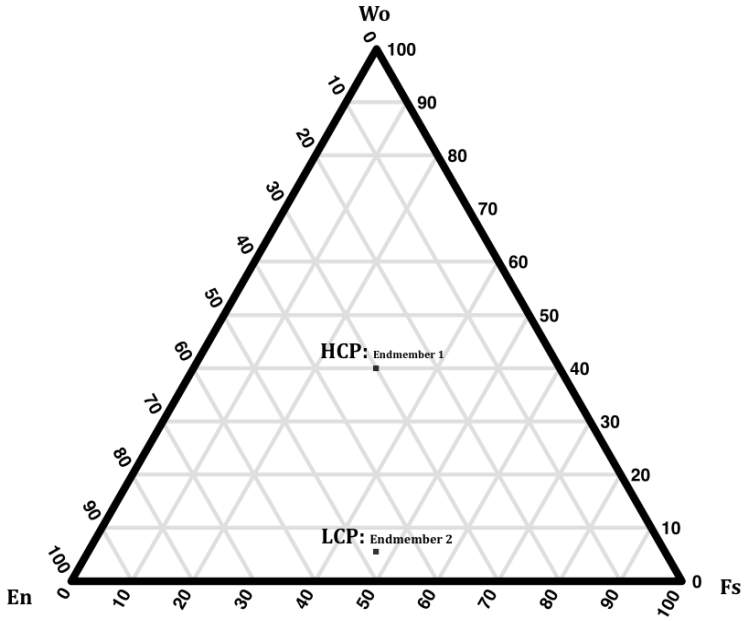

Figure 6: The HCP and LCP Vestan pyroxene endmembers are plotted on a pyroxene quadrilateral. Wo represents wollastonite, En for enstatite, and Fs stands for ferrosilite.

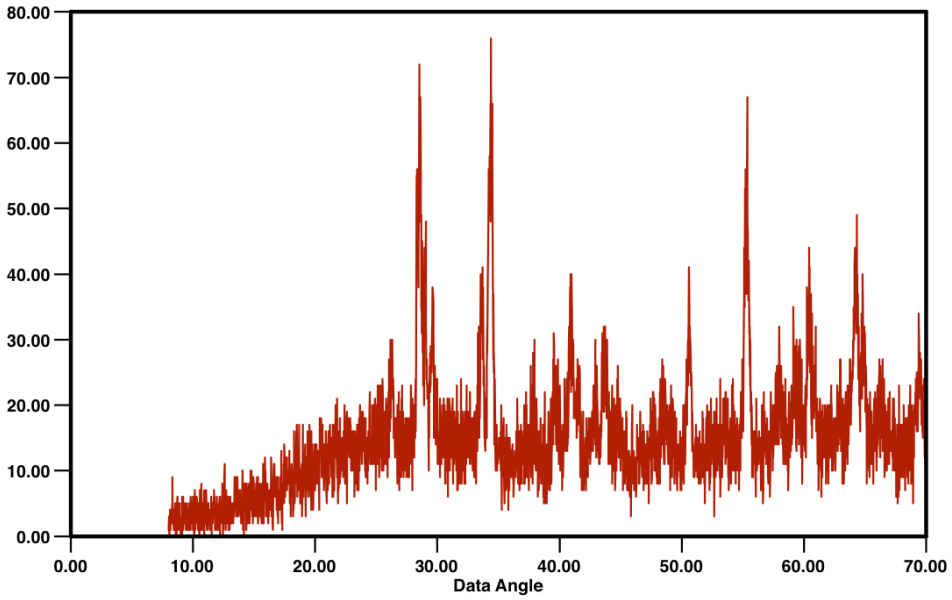

Figure 7: The X-Ray diffraction pattern of the Wo40En30Fs61.5. This pattern shows the lack of emission at the data angle of 10º, which ensures that the pyroxenes were not hydrated and were, indeed, pure.

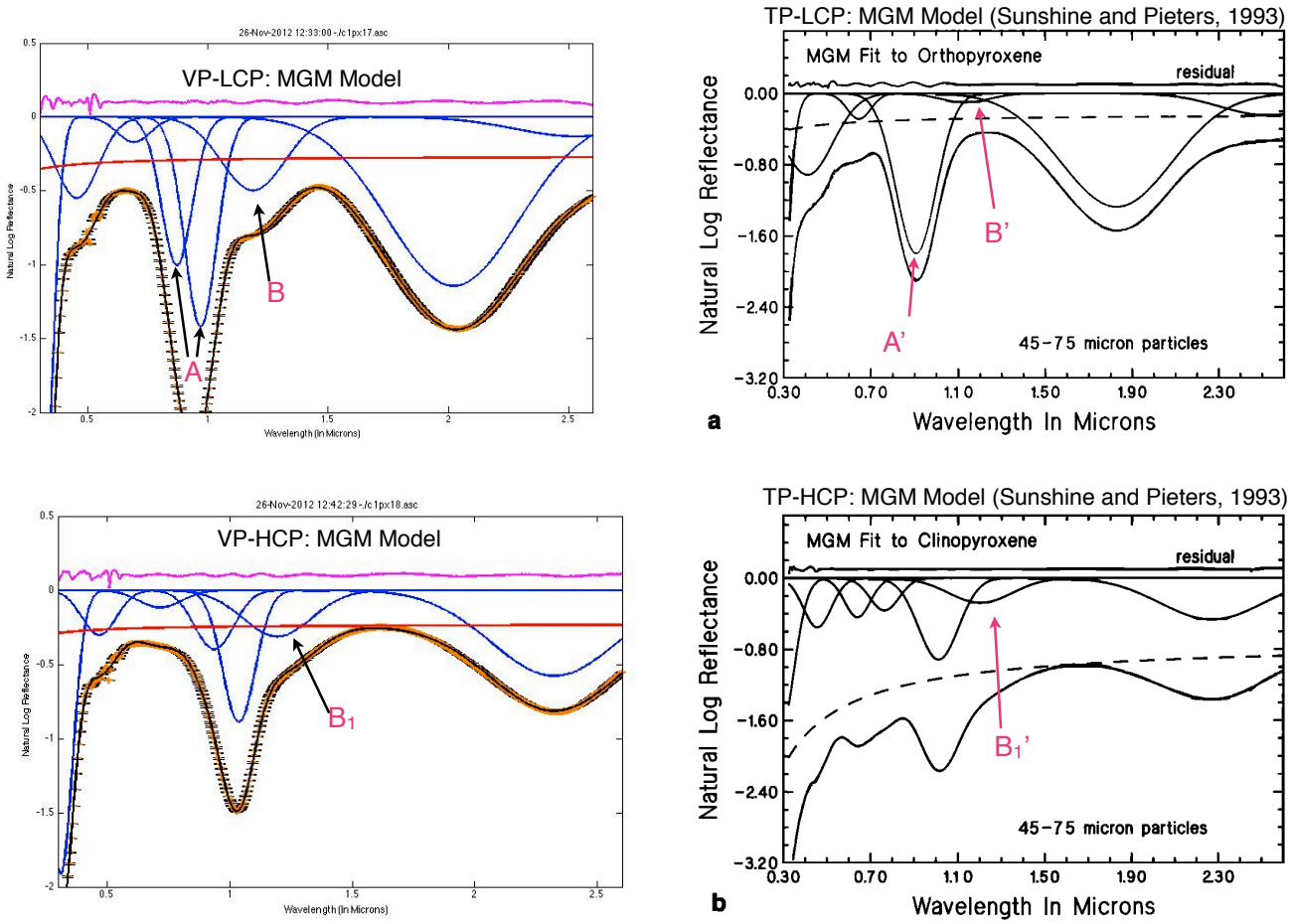

Figure 8: These charts compare the MGM modeling differences between the spectra of terrestrial pyroxene endmembers (TP-HCP, TP-LCP) taken from Sunshine and Pieters (1993) and newly modeled vestan-pyroxene endmembers (VP-HCP, VP-LCP). The pink line represents the rms error, the orange line is the original spectra, the black line is the new fit of that spectra based on the composite absorption bands. The blue gaussian curves are absorption bands and the red line is the continuum.

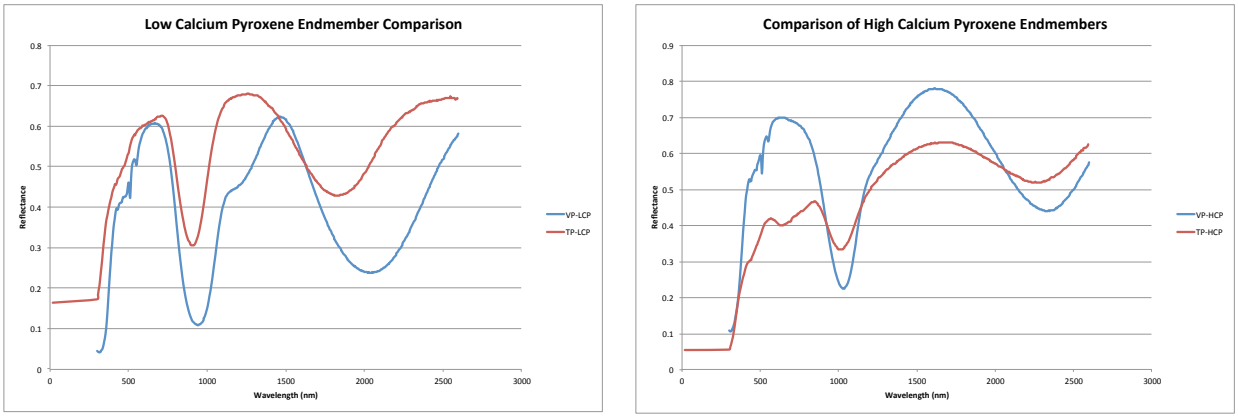

Figure 9: These charts illustrate the differences between the spectra of terrestrial pyroxene endmembers (TP-HCP, TP-LCP) taken from Sunshine and Pieters (1993) and newly modeled vestan-pyroxene endmembers (VP-HCP, VP-LCP).

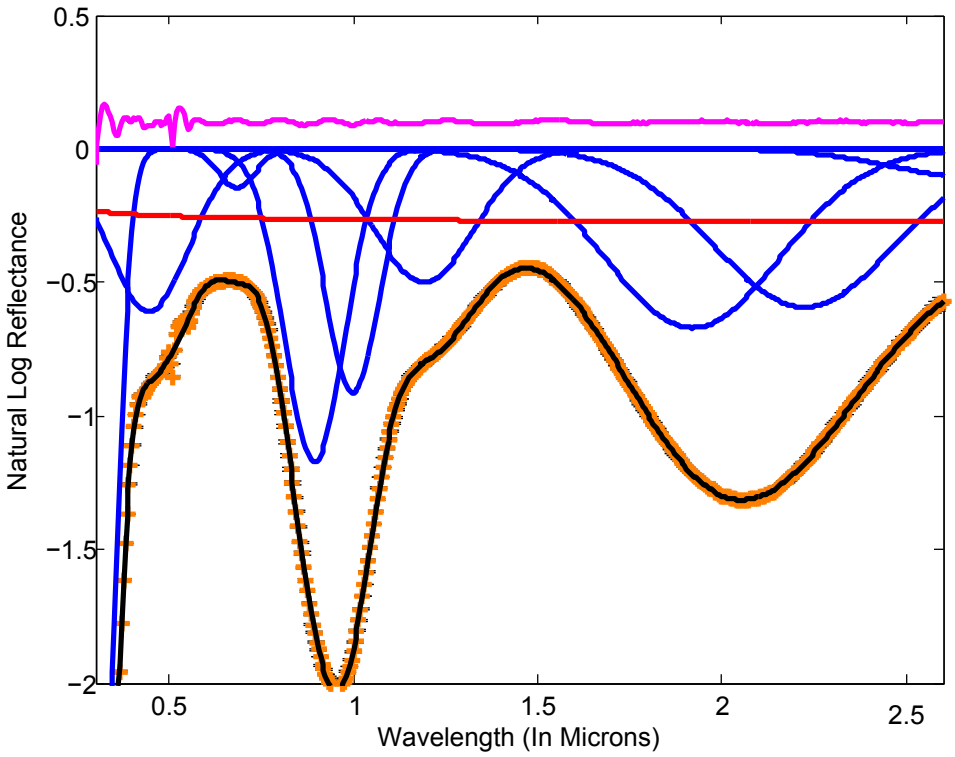

Figure 10: 25%HCP 75%LCP mixture deconvolved.

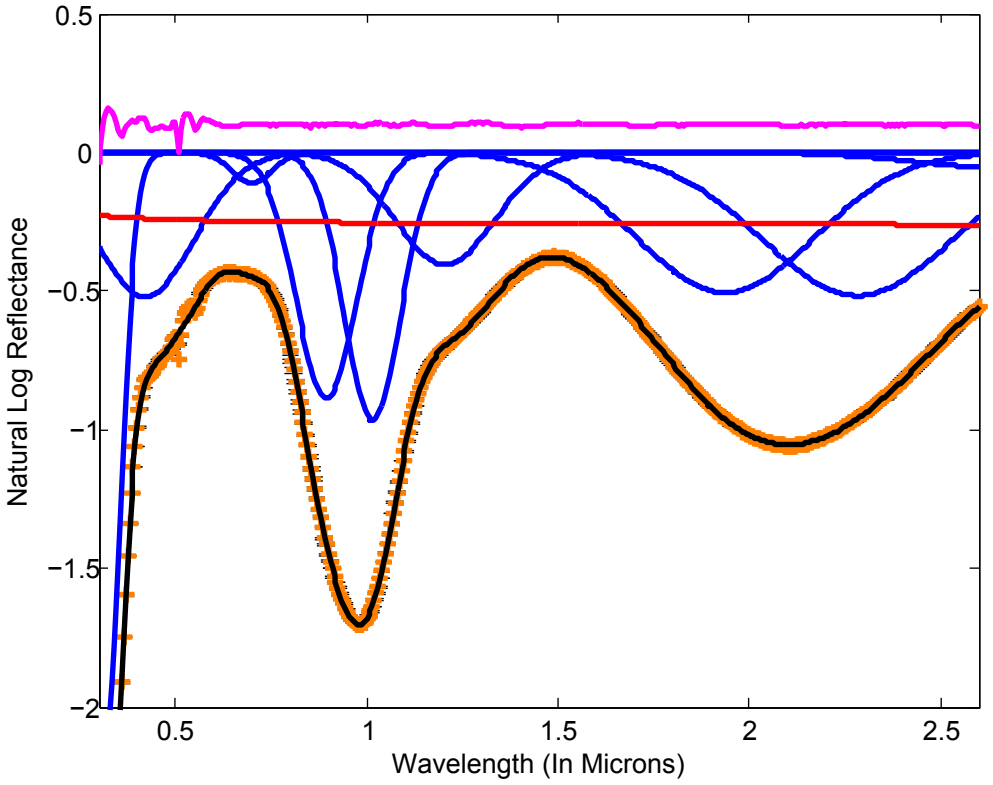

Figure 11: Deconvolution of pyroxene 50%HCP 50%LCP mixture.

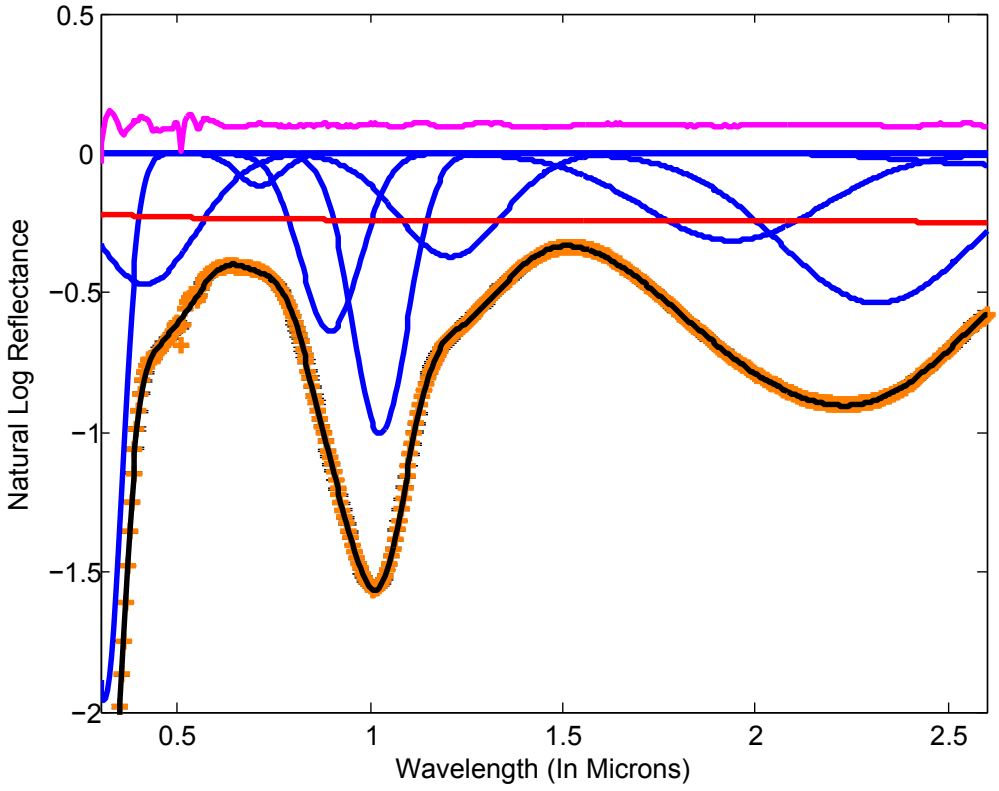

Figure 12: Deconvolution of pyroxene 75%HCP 25%LCP mixture.

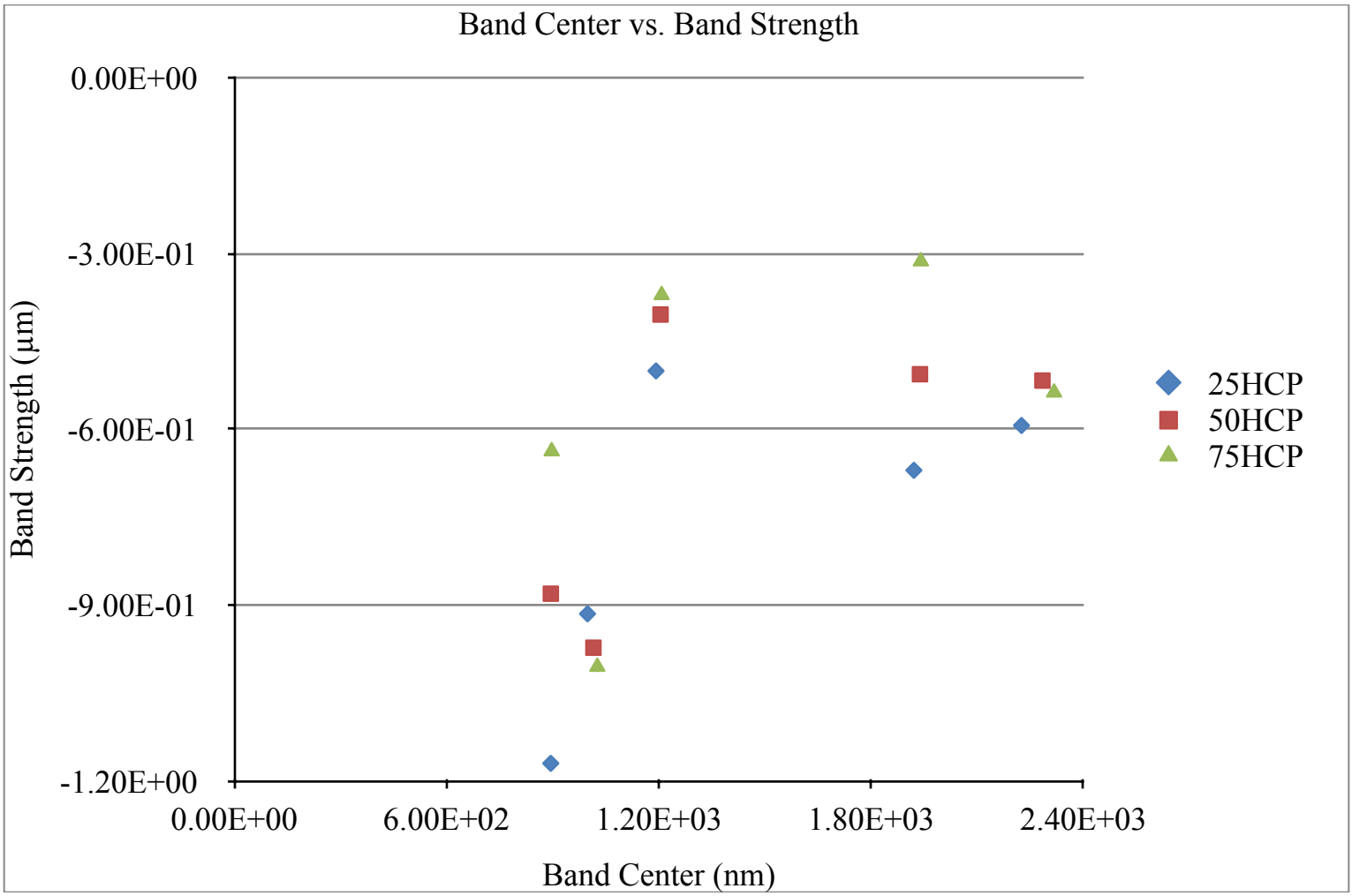

Figure 13: This graph compares band center locations for each of the three mixtures with the absorption band depths. While all of the band center shift slightly to the right with increasing HCP, the shift is subtle. More significant is the difference in band depth between the mixtures. The band depth differences of the 0.9 µm band are especially significant.

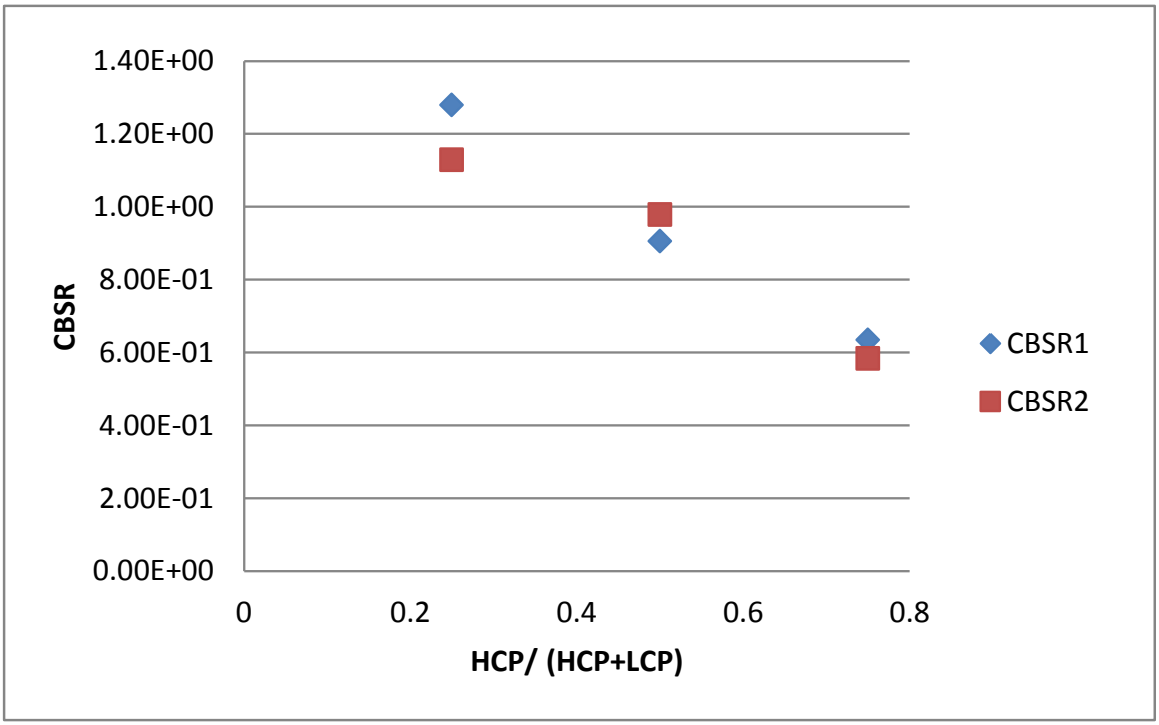

Figure 14: Graph comparing the CBSR (component band strength ratio) to the percent of the pyroxenes that are HCP (HCP/(HCP+LCP)). With the 1µm band strength ratio of HCP and LCP in blue and the 2µm band strength ratio of HCP and LCP in red.

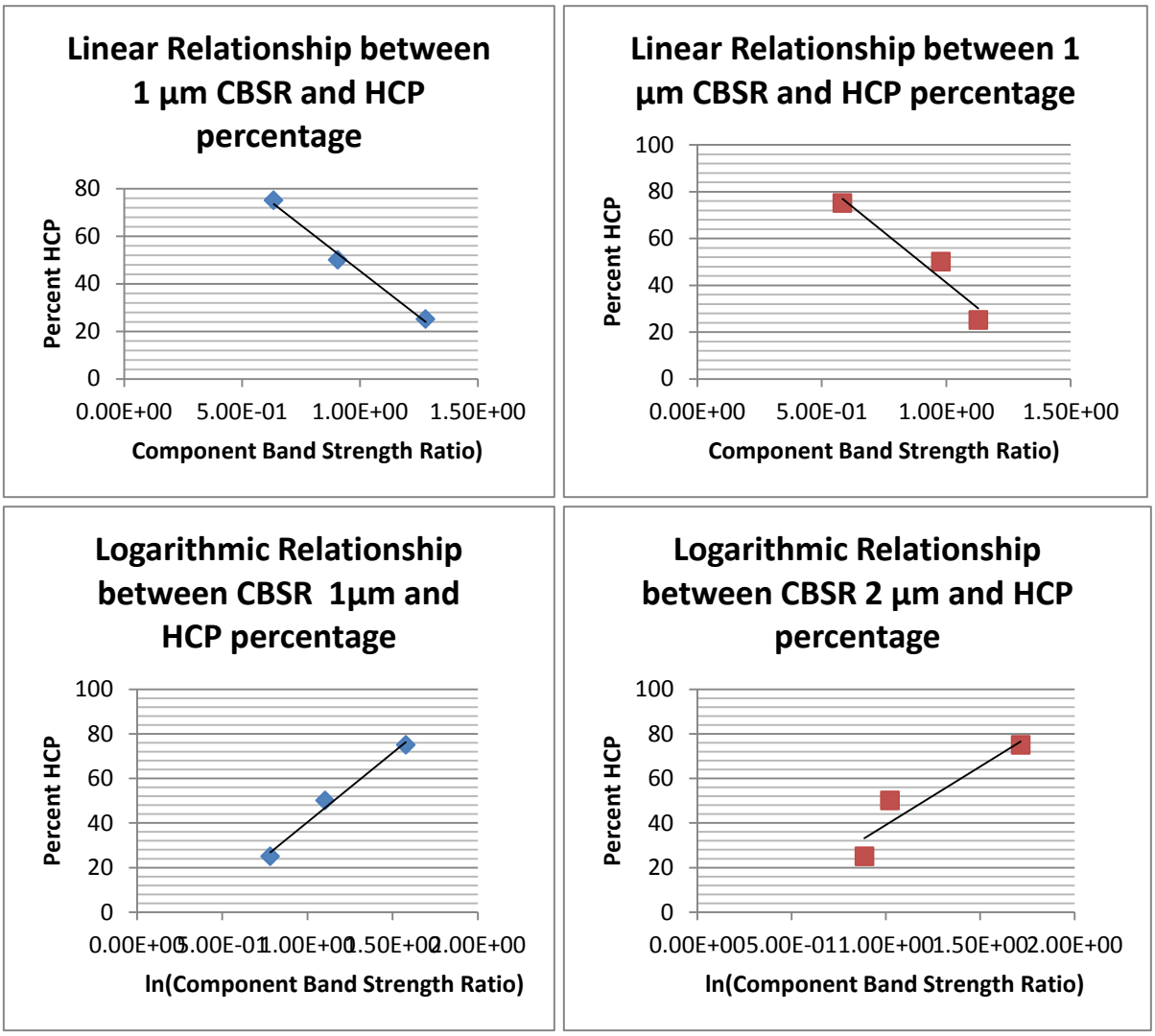

Figure 15: Different relationships between the component band strength ratio between LCP and HCP and the HCP/(HCP+LCP) ratio. Both linear and logarithmic relationships can be made.

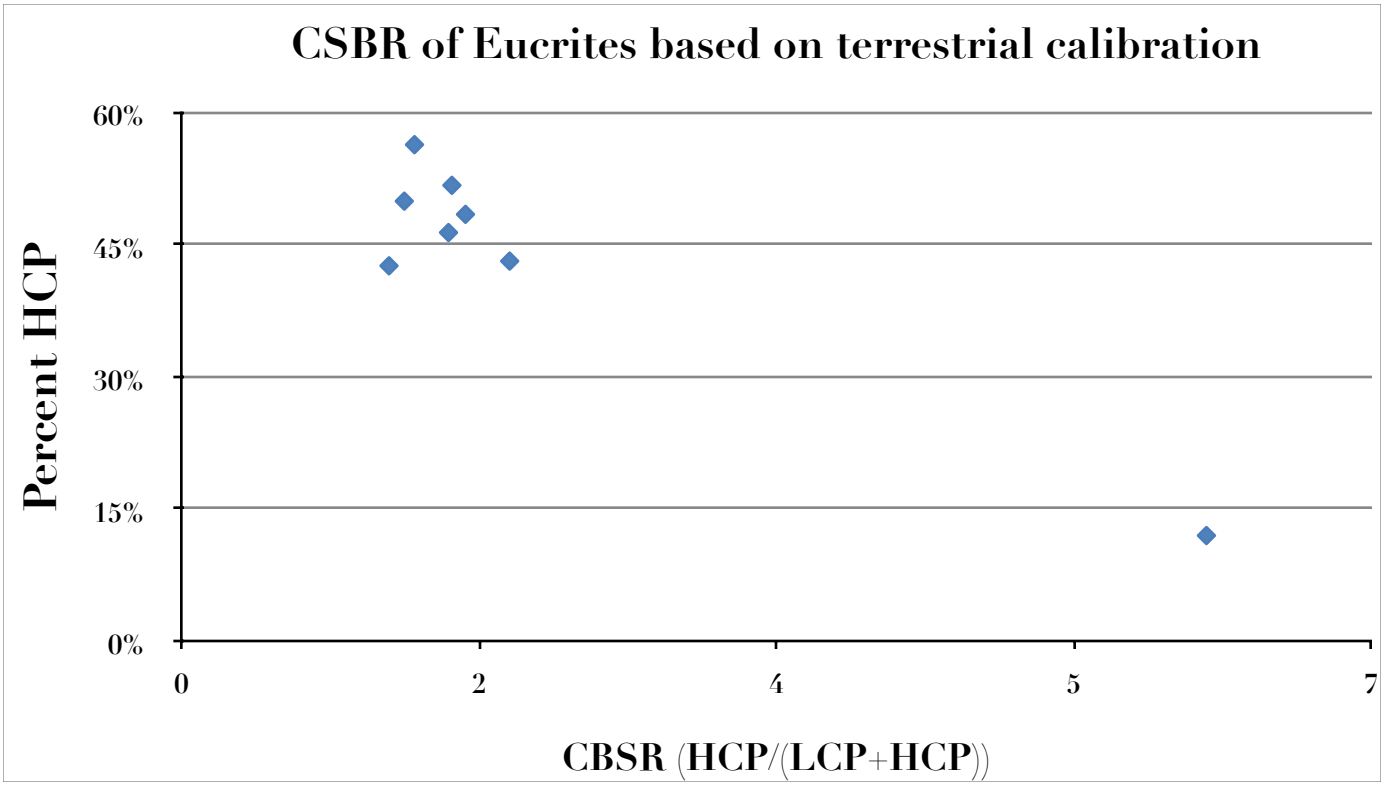

Figure 16: Derived from Mayne et al. (2010), this chart compares the calculated CBSR and known HCP percent for nine eucrites. This graph shows most of these eucrites are clustered around 50% HCP/HCP+LCP . The relationship based on these Eucrites is not clear.

Terrestrial LCP			
Continuum	7.90E-01	-5.55E-06	
(nm)	Center	Width	Strength
Band 1	2.81E+02	9.40E+01	-9.80E-01
Band 2	3.50E+02	3.17E+02	-3.40E-01
Band 3	6.56E+02	1.19E+02	-6.00E-02
Band 4	9.09E+02	1.83E+02	-7.70E-01
Band 5	1.15E+03	2.77E+02	-5.00E-02
Band 6	1.83E+03	5.52E+02	-5.10E-01
Band 7			
Band 8	2.51E+03	5.03E+02	-1.10E-01
rms error,%	0.48		
Terrestrial HCP			
Continuum	6.30E-01	-1.18E-05	
(nm)	Center	Width	Strength
Band 1	2.83E+02	1.06E+02	-1.85E+00
Band 2	4.18E+02	2.12E+02	-3.00E-01
Band 3	6.48E+02	1.21E+02	-2.00E-01
Band 4	7.66E+02	1.54E+02	-1.80E-01
Band 5	1.01E+03	2.00E+02	-5.10E-01
Band 6	1.19E+03	3.21E+02	-1.50E-01
Band 7	2.27E+03	5.33E+02	-2.50E-01
rms error,%	0.60		

Eucrite LCP			
Continuum	7.68E-01	-2.00E-06	
(nm)	Center	Width	Strength
Band 1	3.15E+02	9.54E+01	-2.71E+00
Band 2	4.54E+02	2.10E+02	-5.50E-01
Band 3	6.92E+02	1.69E+02	-1.70E-01
Band 4	8.70E+02	1.52E+02	-1.00E+00
Band 5	9.69E+02	1.59E+02	-1.42E+00
Band 6	1.19E+03	3.09E+02	-5.00E-01
Band 7	2.02E+03	6.46E+02	-1.14E+00
Band 8	2.53E+03	6.10E+02	-1.30E-01
rms error,%	1.18		
Eucrite HCP			
Continuum	7.91E-01	-1.06E-07	
(nm)	Center	Width	Strength
Band 1	3.11E+02	1.16E+02	-1.96E+00
Band 2	4.67E+02	1.68E+02	-3.30E-01
Band 3	7.03E+02	2.02E+02	-1.30E-01
Band 4	9.23E+02	1.91E+02	-3.50E-01
Band 5	1.03E+03	1.62E+02	-9.60E-01
Band 6	1.20E+03	3.31E+02	-3.20E-01
Band 7	2.32E+03	6.13E+02	-5.80E-01
rms error,%	0.97		

Table 1: Comparison between absorption band parameters in a terrestrial LCP and HCP to a Vestan (Eucrite) LCP and HCP. Terrestrial pyroxene chart adapted from Sunshine and Pieters (1993).

25%HCP75%LCP			
Continuum	7.57E-01	1.03E-06	
(nm)	Center	Width	Strength
Band 1	3.14E+02	9.81E+01	-2.57E+00
Band 2	4.45E+02	2.58E+02	-6.07E-01
Band 3	6.84E+02	1.19E+02	-1.45E-01
Band 4	8.94E+02	1.93E+02	-1.17E+00
Band 5	9.98E+02	1.71E+02	-9.14E-01
Band 6	1.19E+03	3.17E+02	-5.00E-01
Band 7	1.92E+03	5.62E+02	-6.70E-01
Band 8	2.22E+03	5.81E+02	-5.93E-01
Band 9	2.70E+03	5.61E+02	-1.10E-01
50%HCP50%LCP			
Continuum	7.67E-01	8.65E-07	
(nm)	Center	Width	Strength
Band 1	3.14E+02	9.79E+01	-2.17E+00
Band 2	4.21E+02	3.02E+02	-5.20E-01
Band 3	7.01E+02	1.25E+02	-1.10E-01
Band 4	8.95E+02	1.85E+02	-8.80E-01
Band 5	1.01E+03	1.74E+02	-9.72E-01
Band 6	1.20E+03	3.07E+02	-4.04E-01
Band 7	1.94E+03	5.50E+02	-5.06E-01
Band 8	2.28E+03	5.89E+02	-5.17E-01
Band 9	2.68E+03	5.62E+02	-5.65E-02
75%HCP25%LCP			
Continuum	7.79E-01	8.00E-07	
(nm)	Center	Width	Strength
Band 1	3.12E+02	1.02E+02	-1.96E+00
Band 2	4.15E+02	3.11E+02	-4.69E-01
Band 3	7.13E+02	1.35E+02	-1.16E-01
Band 4	8.97E+02	1.82E+02	-6.37E-01
Band 5	1.03E+03	1.69E+02	-1.00E+00
Band 6	1.21E+03	3.18E+02	-3.70E-01
Band 7	1.94E+03	5.48E+02	-3.13E-01
Band 8	2.32E+03	5.88E+02	-5.37E-01
Band 9	2.65E+03	5.64E+02	-4.21E-02

Table 2: Compares band parameters of the three mixtures. All mixtures used the same 9 band fit.

	Modal mineralogy measured from thin section						Modal mineralogy calculated from MGM[a]		
	Plag	Pyx	LCP	HCP	Si	OSM	Actual HCP	HCP MGM 1 μm	HCP MGM 2 μm
ALHA81001	61.0	39.0	28.0	11.0	0.0	0.0	28	N/A	N/A
BTN 00300	48.4	45.7	18.7	27.0	4.8	1.0	59	73	71
Chervony Kut	45.0	51.5	22.5	29.0	1.9	1.5	56	61	61
EET 87520	48.5	49.8	28.6	21.2	1.4	0.2	43	65	63
GRA 98098	41.0	50.2	25.9	24.3	8.2	0.6	48	55	59
Ibitira	41.4	53.3	28.6	24.7	4.4	0.9	46	56	44
MAC 02522	41.1	56.6			1.6	0.7	N/A	N/A	N/A
MET 01081	40.3	53.0	25.6	27.4	5.5	1.2	52	55	57
Moore County	43.8	52.2	29.6	22.5	3.4	0.7	43	47	35
PCA 91078	45.7	50.7	25.4	25.3	2.9	0.8	50	63	67
Serra de Magé	52.7	45.1	39.7	5.4	0.7	1.5	12	18	25
Mixture 1							50	50	45
Mixture 2							15	10	19

Note: OSM = Oxides, sulfides, and metal; Si = SiO_2; Plag = plagioclase; Pyx = total pyroxene (LCP + HCP, if present); LCP = low-Ca pyroxene; HCP = high-Ca pyroxene; MGM = modified Gaussian model.
[a]Where % HCP and LCP have been normalized to 100%.

Table 3: From Mayne et al. (2010). Table shows the mineralogy of the Eucrites and the predicted mineralogy of the eucrites from deconvolving their spectra. This table shows how the Earth-based HCP predictions are inaccurate.

	CBSR	HCP Percent Predicted	**HCP Percent**
Chevrony2	137.0%	16.7%	56.3%
EET87520	122.0%	28.3%	42.6%
GRA 98098	167.0%	-6.4%	48.4%
Ibitira	157.0%	1.3%	46.3%
MetO1081	159.0%	-0.2%	51.7%
Moore	193.0%	-26.4%	43.1%
PCA 91078	131.0%	21.4%	49.9%
Serra de Mag	603.0%	-342.1%	12.0%

Table 4: Comparison with Mayne et al. (2010) derived CBSR (component band strength ratio), known eucrite high calcium pyroxene percent (HCP/(HCP+LCP)), and predicted HCP percent.

REFERENCES

Adams J. B. 1974. Visible and near-infrared diffuse reflectance spectra of pyroxenes as applied to remote sensing of solid objects in the solar system. *Journal of Geophysical Research* 79: 4829–4836.

Anovitz L. M., Essene E. J., and Dunham W. R. 1988. Order-disorder experiments on orthopyroxene: Implications for the orthopyroxene geospeedometer. *American Mineralogist* 73: 1060–1073.

Beck, P., J. -A Barrat, F. Grisolle, E. Quirico, B. Schmitt, F. Moynier, P. Gillet, and C. Beck. 2011. NIR spectral trends of HED meteorites: Can we discriminate between the magmatic evolution, mechanical mixing and observation geometry effects? *Icarus* 216, no. 2: 560-571.

Burns R. G. 1993. *Mineralogical applications of crystal field theory*. Cambridge: Cambridge University Press. 551 p.

Binzel R. P., Gaffey M. J., Thomas P. T., Zellner B. H., Storrs A. D., and Wells E. N. 1997. Geologic mapping of Vesta from 1994 Hubble Space Telescope images. *Icarus* 128:95–103.

Cloutis E. A. and Gaffey M. J. 1991a. Pyroxene spectroscopy revisited—Spectral-compositional correlations and relationship to geothermometry. *Journal of Geophysical Research* 96: 22, 809–22, 826.

Cloutis E. A. and Gaffey M. J. 1991b. Spectral-compositional variations in the constituent minerals of mafic and ultramafic assemblages and remote-sensing implications. *Earth, Moon, and Planets* 53: 11–53.

Cloutis E. A. 2002. Pyroxene reflectance spectra: Minor absorption bands and effects of elemental substitutions. *Journal of Geophysical Research* 107:E6,

doi:10.1029/2001/JE001590.

Ghosh, Amitabha and Harry Y. McSween Jr. 1998. A thermal model for the differentiation of asteroid 4 vesta, based on radiogenic heating. *Icarus* 134, no. 2: 187-206.

Haack, H., Rasmussen, K.L., and Warren, P.H. 1990. Effects of regolith/megaregolith insulation on the cooling histories of differentiated asteroids. *Journal of Geophysical Research: Solid Earth.* 95: 5111-5124. doi: 10.1029/JB095iB04p05111.

Klima R. L., Pieters C. M., and Dyar M. D. 2007. Spectroscopy of synthetic Mg-Fe pyroxenes I: Spin-allowed and spin-forbidden crystal field bands in the visible and near-infrared. *Meteoritics & Planetary Science* 42:235–253.

Klima R. L., Pieters C. M., and Dyar M. D. 2008. Characterization of the 1.2 μm M1 pyroxene band: Extracting cooling history from near-IR spectra of pyroxenes and pyroxene-dominated rocks. *Meteoritics & Planetary Science* 43:1591–1604.

Klima R. L., Dyar M. D, and Pieters C. M. 2011. Near-infrared spectra of clinopyroxenes: Effects of calcium content and crystal structure. *Meteoritics & Planetary Science* 46:379–395.

Lindsley D. H. 1983. Pyroxene thermometry. *American Mineralogist* 68:477–493.

Molin G. and Zanazzi P. F. 1991. Intracrystalline Fe^{2+}-Mg ordering in augite: Experimental study and geothermometric applications. *European Journal of Mineralogy* 3: 863–875.

Mason B. 1962. *Meteorites*. New York: J. Wiley and Sons.

Mayne R. G., McSween H. Y., McCoy T. J., and Gale A. 2009. Petrology of the unbrecciated eucrites. *Geochimica et Cosmochimica Acta* 73:794–819.

Mayne, R. G., Sunshine, J. M., McSween, H. Y., McCOY, T. J., CORRIGAN, C. M. and GALE, A. 2010 Petrologic insights from the spectra of the unbrecciated eucrites: Implications for Vesta and basaltic asteroids. Meteoritics & Planetary Science,

45: 1074–1092. doi: 10.1111/j.1945-5100.2010.01090.

McCord T. B., Adams J. B., and Johnson T. V. 1970. Asteroid Vesta: Spectral reflectivity and compositional implications. *Science* 168:1445–1447.

McCoy T. J., Mittlefehldt D. W., and Wilson L. 2006. Asteroid differentiation. In *Meteorites and the early solar system II*, edited by LaurettaD. S. and McSweenH. Y.Jr. Tucson, AZ: The University of Arizona Press. pp. 733–746.

McSween, H., Jr., Mittlefehldt, D., Beck, A., Mayne, R., and McCoy, T. 2011. HED Meteorites and Their Relationship to the Geology of Vesta and the Dawn *Mission: Space Science Reviews* 163:141-174, doi: 10.1007/s11214-010-9637-z.

Mittlefehldt, David W. and Marilyn M. Lindstrom. 1997. Magnesian basalt clasts from the EET 92014 and kapoeta howardites and a discussion of alleged primary magnesian HED basalts. *Geochimica Et Cosmochimica Acta* 61, no. 2: 453-462.

Molin G. and Zanazzi P. F. 1991. Intracrystalline Fe^{2+}-Mg ordering in augite: Experimental study and geothermometric applications. *European Journal of Mineralogy* 3: 863–875.

Pieters C. M. and Hiroi T. 2004. RELAB (Reflectance Experiment Laboratory): A NASA multi-user spectroscopy facility (abstract #1720). 35th Lunar and Planetary Science Conference. CD-ROM.

Pun A. and Papike J. J. 1996. Unequilibrated eucrites and the equilibrated Juvinas eucrite: Pyroxene REE systematics and major, minor, and trace element zoning. *American Mineralogist* 81:1438–1451.

Righter K. and Drake M. J. 1997. A magma ocean on Vesta: Core formation and petrogenesis of eucrites and diogenites. *Meteoritics & Planetary Science* 32:929–944.

Rossman G. R. 1980. Pyroxene spectroscopy. In *Pyroxenes*, edited by PrewittC. Reviews

of Mineralogy, vol. 7. Washington, D.C.: Mineralogical Society of America. pp. 95–115.

Russell C. T., Coradini A., Christensen U., De Sanctis M. C., Feldman W. C., Jaumann R., Keller H. U., Konopliv A., McCord T. B., McFadden L. A., McSween H. Y., Mottola S., Neukum G., Pieters C. M., Prettyman T. H., Raymond C. A., Smith D. E., Sykes M. V., Williams B., Wise J., and Zuber M. T. 2004. Dawn: A journey in space and time. *Planetary and Space Science* 52:465–489.

Russell C. T., Capaccioni F., Coradini A., Christensen U., De Sanctis M. C., Feldman W. C., Jaumann R., Keller H. U., Konopliv A., McCord T. B., McFadden L. A., McSween H. Y., Mottola S., Neukum G., Pieters C. M., Prettyman T. H., Raymond C. A., Smith D. E., Sykes M. V., Williams B., and Zuber M. T. 2006. Dawn discovery mission to Vesta and Ceres: Present status. *Advances in Space Research* 38:2043–2048.

Ruzicka A., Synder G. A., and Taylor L. A. 1997. Vesta as the howardite, eucrite, and diogenite parent body: Implications for the size of a core and for large-scale differentiation. *Meteoritics & Planetary Science* 32:825–840.

Saxena S. K., Ghose S., and Turnock A. C. 1974. Cation distribution in low-calcium pyroxenes: Dependence on temperature and calcium content and the thermal history of lunar and terrestrial pigeonites. *Earth and Planetary Science Letters* 21: 194–200.

Stolper E. 1977. Experimental petrology of eucritic meteorites. *Geochimica et Cosmochimica Acta* 41:587–611.

Sunshine J. M. and Pieters C. M. 1993. Estimating modal abundances from the spectra of natural and laboratory pyroxene mixtures using the modified Gaussian model. *Journal of Geophysical Research* 98: 9075–9087.

Sunshine J. M., Pieters C. M., and Pratt S. F. 1990. Deconvolution of mineral absorption bands—An improved approach. *Journal of Geophysical Research* 95: 6955–6966.

Sunshine J. M., Pieters C. M., Pratt S. F., and McNaron-Brown K. S. 1999. Absorption band modeling in reflectance spectra: Availability of the modified Gaussian model (abstract #1306). 30th Lunar and Planetary Science Conference. CD-ROM.

Sunshine J. M., Bus S. J., McCoy T. J., Burbine T. H., Corrigan C. M., and Binzel R. P. 2004. High-calcium pyroxene as an indicator of differentiation in asteroids and meteorites. *Meteoritics & Planetary Science* 39:1343–1357.

Tarantola, A., B. Valette, Generalized non-linear inverse problems solved using the least squares criterion, *Rev. Geophys.*, 20, 219–232, 1982.

Virgo D. and Hafner S. S. 1970. Fe^{2+}, Mg order-disorder in natural orthopyroxenes. *American Mineralogist* 55: 201–223.

M. Wadhwa, G. Srinivasan, R.W. Carlson, in *Meteorites and the Early Solar System II*, ed. by D.S. Lauretta, H.Y. McSween (University of Arizona Press, Tucson, 2006), p. 715